

Analytic solution of Timoshenko beam excited by real seismic support motions

Yong-Woo Kim*

Department of Mechanical Engineering, Suncheon National University, Jungangro 255, Suncheon, Jeonnam 57922, Republic of Korea

(Received June 30, 2016, Revised December 23, 2016, Accepted February 10, 2017)

Abstract. Beam-like structures such as bridge, high building and tower, pipes, flexible connecting rods and some robotic manipulators are often excited by support motions. These structures are important in machines and structures. So, this study proposes an analytic method to accurately predict the dynamic behaviors of the structures during support motions or an earthquake. Using Timoshenko beam theory which is valid even for non-slender beams and for high-frequency responses, the analytic responses of fixed-fixed beams subjected to a real seismic motions at supports are illustrated to show the principled approach to the proposed method. The responses of a slender beam obtained by using Timoshenko beam theory are compared with the solutions based on Euler-Bernoulli beam theory to validate the correctness of the proposed method. The dynamic analysis for the fixed-fixed beam subjected to support motions gives useful information to develop an understanding of the structural behavior of the beam. The bending moment and the shear force of a slender beam are governed by dynamic components while those of a stocky beam are governed by static components. Especially, the maximal magnitudes of the bending moment and the shear force of the thick beam are proportional to the difference of support displacements and they are influenced by the seismic wave velocity.

Keywords: Timoshenko beam; support motions; eigenfunction expansion method; time-dependent boundary condition; quasi-static decomposition method; static component-dominated beam

1. Introduction

Beam-like structures or structural members are often excited by the motions at supports or connections, e.g., piping system in nuclear power plants subjected to support motions at their connections to containment buildings and heavy equipment, long and slender structures such as chimneys, towers, long bridges and oil pipeline subjected to ground motions. They can be modeled as Euler-Bernoulli beam subjected to multi-support motions if the foundation or ground soil is assumed to be rigid. However, a flexible connecting rod, some robotic manipulators, and some pipes in nuclear power plants are not slender beams but rather stocky ones. They are often excited by the motions transmitted from connections or supports in main structures or foundation. Thus, it is necessary to employ Timoshenko beam that can represent both of slender one and stocky one. Therefore, the vibration associated with Timoshenko beam subjected to support motions is to be considered in this investigation.

The vibration of the aforementioned beams is characterized as the problem of flexural vibration with time-dependent boundary conditions. Mindlin and Goodman (1950) developed the quasi-static decomposition method for Euler-Bernoulli beam and applied it to obtain a solution of the problem. Many researchers have applied it to the

analysis of structures subjected to multiple support excitations by using various approaches such as time history analysis, response spectrum method of analysis or frequency domain spectral analysis (Masri 1976, Abel-Ghaffar and Rood 1982, Clough *et al.* 1993, Chopra 1995, Yau *et al.* 2007, Frýba *et al.* 2009, Yau 2009, Zhang *et al.* 2009, Datta, 2010, Liu *et al.* 2011, and Kim *et al.* 2013, 2015, 2016).

As for Timoshenko beam subjected to support motions, there are not so many papers compared with those on Euler-Bernoulli beam. Lee and Lin (1998) presented a solution procedure for elastically restrained non-uniform Timoshenko beams by generalizing the quasi-static decomposition method. But there is a remark that such a description concerns only for elastically restrained Timoshenko beams and they did not treat the Timoshenko beam subjected to support motions. Kim (2016) proposed a solution procedure for responses of simply-supported Timoshenko beams subjected to support motions using eigenfunction expansion method. He applied the quasi-static decomposition method to the system of the second order differential equations of the beams to resolve the difficulties of time-dependent boundary conditions.

The eigenvalues of Timoshenko beam and the beam vibrations have been studied over the years by many investigators (Han *et al.* 1999, Stephen *et al.* 2006, Rensburg *et al.* 2006, Majkut 2009, Díaz-de-Anda *et al.* 2012, and Li *et al.* 2014). Han *et al.* (1999) presented systematic analysis of four models such as Euler-Bernoulli, Rayleigh, shear and Timoshenko beams. They presented the orthogonal conditions of the eigenfunctions and the

*Corresponding author, Professor
E-mail: kyw@sunchon.ac.kr

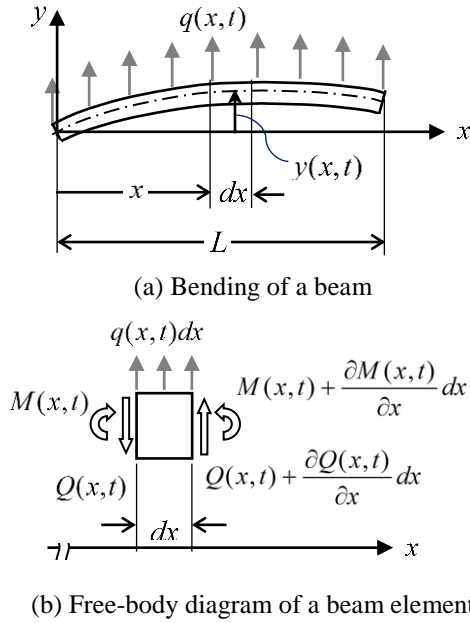


Fig. 1 Beam in flexure

procedure to obtain the forced response using the method of eigenfunction expansion. Recently, Rensburg *et al.* (2006) presented a mathematically systematic approach to solving the eigenvalue problems associated with the uniform Timoshenko beam model, of which the results are identical to those of Han *et al.* (1999).

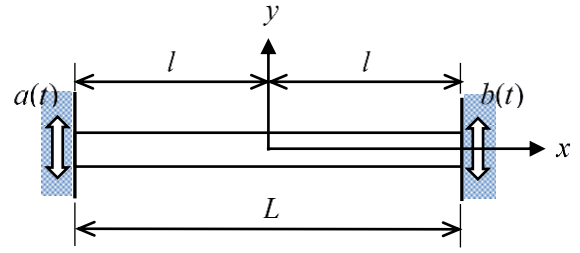
Though the method of eigenfunction expansion is valid for the beams with typical or classical boundary conditions, a fixed-fixed beam is chosen for analysis in this paper because such a beam is frequently used in nuclear power plants. For example, the pipes connecting between reactor pressure vessel and steam generators or between reactor pressure vessel and reactor coolant pumps are considered as a thick beam. Since the bending moment and shear force are main concerns in structural design, dynamic analysis focusing on the structural loads is carried out by using the proposed method. To check the correctness of the proposed method, the dynamic responses of Timoshenko beam are compared with those obtained by Euler-Bernoulli beam theory. The comparison shows that their solutions match well. The dynamic analysis for the fixed-fixed beam subjected to support motions gives useful information to develop an understanding of the structural behavior of the beam. The information or findings are reported in this paper.

2. Timoshenko beam subjected to support motions

The motion of Timoshenko beam with uniform cross section is described by

$$\begin{cases} \rho A \ddot{y}(x,t) - \kappa GA \{y''(x,t) - \theta'(x,t)\} = q(x,t) \\ \rho I \ddot{\theta}(x,t) - EI \theta''(x,t) - \kappa GA \{y'(x,t) - \theta(x,t)\} = 0 \end{cases} \quad (1)$$

where $y(x,t)$ is the transverse displacement at a point x and time t , $\theta(x,t)$ is the angle of the rotation of a cross section,

Fig. 2 A fixed-fixed beam subjected to the support displacements, $a(t)$ at the left end and $b(t)$ at the right end

and $q(x,t)$ is the transverse force per unit length as shown in Fig. 1(a). A superimposed dot denotes a time derivative and a superscript prime stands for a spatial differentiation. EI , ρA , L and κ denote the flexural rigidity, mass per unit length, the length of the beam and the shear correction factor, respectively. For simplicity, but without loss of generality, assume the load $q(x,t)$ be zero during support motions. The following constitutive equations for the moment $M(x,t)$ and the shear force $Q(x,t)$ shown in Fig. 1(b) are used to derive the governing equations.

$$\begin{aligned} M(x,t) &= EI \theta'(x,t) \\ Q(x,t) &= \kappa GA \{y'(x,t) - \theta(x,t)\} \end{aligned} \quad (2)$$

Consider a fixed-fixed beam in Fig. 2 for illustration. The boundary conditions of the fixed-fixed beam are

$$y(-l,t) = a(t), \quad y(l,t) = b(t), \quad \theta(-l,t) = 0, \quad \theta(l,t) = 0 \quad (3)$$

where $a(t)$ and $b(t)$ are support displacements prescribed by records of support motion.

Assuming that the motion starts from rest, the initial conditions are

$$y(x,0) = 0, \quad \dot{y}(x,0) = 0, \quad \theta(x,0) = 0, \quad \dot{\theta}(x,0) = 0 \quad (4)$$

2.1 Quasi-static displacements

By the quasi-static decomposition method, the total displacements of $y(x,t)$ and $\theta(x,t)$ are decomposed into two parts

$$\begin{cases} y(x,t) \\ \theta(x,t) \end{cases} = \begin{cases} y_s(x,t) \\ \theta_s(x,t) \end{cases} + \begin{cases} w(x,t) \\ \phi(x,t) \end{cases} \quad (5)$$

where $y_s(x,t)$ and $\theta_s(x,t)$ are quasi-static linear displacement and quasi-static angular displacement, respectively, $w(x,t)$ and $\phi(x,t)$ are dynamic contributions. The quasi-static parts should satisfy the following partial differential equations

$$\begin{cases} \kappa GA (y_s'' - \theta_s') = 0 \\ EI \theta_s'' + \kappa GA (y_s' - \theta_s) = 0 \end{cases} \quad (6)$$

and the boundary conditions including non-homogeneous ones

$$\begin{aligned} y_s(-l,t) &= a(t), \\ y_s(l,t) &= b(t), \\ \theta_s(-l,t) &= 0, \\ \theta_s(l,t) &= 0. \end{aligned} \quad (7)$$

Solving Eq. (6) directly by using the boundary conditions, we obtain following solutions.

$$\begin{aligned} y_s(x,t) &= L_1(x) \cdot a(t) + L_2(x) \cdot b(t) \\ \theta_s(x,t) &= R_1(x) \cdot a(t) + R_2(x) \cdot b(t) \end{aligned} \quad (8)$$

where

$$\begin{aligned} L_1(x) &= \frac{1}{(1+3K)} \left\{ \frac{1}{4l^3} x^3 - \frac{3}{4l} (1+2K)x \right\} + \frac{1}{2} \\ L_2(x) &= \frac{1}{(1+3K)} \left\{ -\frac{1}{4l^3} x^3 + \frac{3}{4l} (1+2K)x \right\} + \frac{1}{2} \\ R_1(x) &= -R_2(x) = \frac{3}{4} \cdot \frac{1}{(1+3K)} \left(\frac{1}{l^3} x^2 - \frac{1}{l} \right) \end{aligned} \quad (9)$$

In the above equation (9), K is defined as

$$K = \frac{EI}{\kappa GA l^2} \quad (10)$$

2.2 Dynamic displacements

For free vibration, the equation of motion in Eq. (1) can be rewritten in terms of the dynamic displacements

$$\begin{cases} \rho A \ddot{w} - \kappa GA (w'' - \phi') = -\rho A \ddot{y}_s \\ \rho I \ddot{\phi} - EI \phi'' - \kappa GA (w' - \phi) = -\rho I \ddot{\theta}_s \end{cases} \quad (11)$$

or, in matrix form

$$[M]\{\ddot{v}\} + [L]\{v\} = \{f\} \quad (12)$$

where

$$\begin{aligned} [M] &= \begin{bmatrix} \rho A & 0 \\ 0 & \rho I \end{bmatrix}, \\ [L] &= \begin{bmatrix} -\kappa GA \frac{d^2}{dx^2} & \kappa GA \frac{d}{dx} \\ -\kappa GA \frac{d}{dx} & -EI \frac{d^2}{dx^2} + \kappa GA \end{bmatrix}, \\ \{v\} &= \begin{Bmatrix} w(x,t) \\ \phi(x,t) \end{Bmatrix}, \\ \text{and} \\ \{f\} &= \begin{Bmatrix} -\rho A \ddot{y}_s(x,t) \\ -\rho I \ddot{\theta}_s(x,t) \end{Bmatrix}. \end{aligned} \quad (13)$$

The boundary conditions corresponding to Eq. (7) are rewritten in terms of dynamic components as follows

$$\begin{aligned} w(-l,t) &= 0, \\ w(l,t) &= 0, \\ \phi(-l,t) &= 0, \\ \phi(l,t) &= 0. \end{aligned} \quad (14)$$

The initial conditions of Eq. (11) are also written as follows

$$\begin{aligned} w(x,0) &= -y_s(x,0), \\ \dot{w}(x,0) &= -\dot{y}_s(x,0), \\ \phi(x,0) &= -\theta_s(x,0), \\ \dot{\phi}(x,0) &= -\dot{\theta}_s(x,0). \end{aligned} \quad (15)$$

2.2.1 General form of solutions

Using the method of eigenfunction expansion method, we can obtain the solutions of Eq. (11), i.e., $w(x,t)$ and $\phi(x,t)$ that satisfy relevant boundary conditions and initial conditions.

At first, consider the eigenvalue problem of Eq. (12)

$$[M]\{\ddot{v}\} + [L]\{v\} = \{0\} \quad (16)$$

The solutions of Eq. (16) are separable in space and time. Thus, assume $w(x,t)$ and $\phi(x,t)$ as follows.

$$\begin{cases} w(x,t) = W(x)T(t) \\ \phi(x,t) = \Phi(x)T(t) \end{cases} \quad (17)$$

With such an assumption, Eq. (16) can be written as

$$([L] - \omega^2 [M])\{V\} = \{0\} \quad (18)$$

where ω is the frequency of $T(t)$, and $\{V\}^T = \{W(x) \Phi(x)\}$. Assuming the form of $\{V\}$ as

$$\{V\} = \begin{Bmatrix} W(x) \\ \Phi(x) \end{Bmatrix} = \begin{Bmatrix} Y_1 \\ Y_2 \end{Bmatrix} e^{qx} \quad (19)$$

where Y_1 and Y_2 are arbitrary constants.

Han *et al.* (1999) and Rensburg *et al.* (2006) obtained the following solutions of Eq. (16).

$$\{V\} = \begin{Bmatrix} W(x) \\ \Phi(x) \end{Bmatrix} = \begin{Bmatrix} q \\ q^2 + \beta^2 \end{Bmatrix} e^{qx} \quad (20)$$

where

$$q^2 = \frac{1}{2} (-d \pm \sqrt{\Delta}) \quad \text{and} \quad \beta^2 = \frac{\rho A}{\kappa GA} \omega^2 \quad (21)$$

In Eq. (21), d and Δ are defined as follows

$$\begin{aligned} d &= \left(\frac{\rho I}{EI} + \frac{\rho A}{\kappa GA} \right) \omega^2 \quad \text{and} \\ \Delta &= d^2 - 4 \frac{\rho A}{\kappa GA} \cdot \frac{\rho I}{EI} \omega^2 \left(\omega^2 - \frac{\kappa GA}{\rho I} \right). \end{aligned} \quad (22)$$

Using Eq. (20), we obtain the solutions of Eq. (18) after several manipulations, as follows:

• When $\omega^2 < \kappa GA/\rho I$

$$\begin{aligned} \begin{Bmatrix} W(x) \\ \Phi(x) \end{Bmatrix} &= A \begin{Bmatrix} \frac{\sinh(r_1 x)}{\beta^2 + (r_1)^2} \cosh(r_1 x) \\ \frac{\cosh(r_1 x)}{r_1} \sinh(r_1 x) \end{Bmatrix} \\ &+ B \begin{Bmatrix} \frac{\cosh(r_1 x)}{\beta^2 + (r_1)^2} \sinh(r_1 x) \\ \frac{\sinh(r_1 x)}{r_1} \cosh(r_1 x) \end{Bmatrix} \\ &+ C \begin{Bmatrix} \frac{\sin(r_2 x)}{\beta^2 - (r_2)^2} \cos(r_2 x) \\ -\frac{\cos(r_2 x)}{r_2} \sin(r_2 x) \end{Bmatrix} \\ &+ D \begin{Bmatrix} \frac{\cos(r_2 x)}{\beta^2 - (r_2)^2} \sin(r_2 x) \\ \frac{\sin(r_2 x)}{r_2} \cos(r_2 x) \end{Bmatrix} \end{aligned} \quad (23)$$

where A , B , C , and D are arbitrary constants and r_1 and r_2 are

$$r_1 = \left\{ \frac{1}{2}(-d + \sqrt{\Delta}) \right\}^{1/2} \quad \text{and} \quad r_2 = \left\{ \frac{1}{2}(d + \sqrt{\Delta}) \right\}^{1/2} \quad (24)$$

• When $\omega^2 > \kappa GA/\rho I$

$$\begin{aligned} \begin{Bmatrix} W(x) \\ \Phi(x) \end{Bmatrix} = & E \begin{Bmatrix} \sin(p_1 x) \\ -\frac{\beta^2 - (p_1)^2}{p_1} \cos(p_1 x) \end{Bmatrix} \\ & + F \begin{Bmatrix} \cos(p_1 x) \\ \frac{\beta^2 - (p_1)^2}{p_1} \sin(p_1 x) \end{Bmatrix} \\ & + G \begin{Bmatrix} \sin(p_2 x) \\ -\frac{\beta^2 - (p_2)^2}{p_2} \cos(p_2 x) \end{Bmatrix} \\ & + H \begin{Bmatrix} \cos(p_2 x) \\ \frac{\beta^2 - (p_2)^2}{p_2} \sin(p_2 x) \end{Bmatrix} \end{aligned} \quad (25)$$

where E , F , G , and H are arbitrary constants and p_1 and p_2 are

$$p_1 = \left\{ \frac{1}{2}(d - \sqrt{\Delta}) \right\}^{1/2} \quad \text{and} \quad p_2 = \left\{ \frac{1}{2}(d + \sqrt{\Delta}) \right\}^{1/2} \quad (26)$$

2.2.2 Frequency equations and normalized modes

Using the boundary conditions in Eq. (14), we can obtain the following two frequency equations, i.e., one for $\omega^2 < \kappa GA/\rho I$ and the other for $\omega^2 > \kappa GA/\rho I$.

For $\omega^2 < \kappa GA/\rho I$, the frequency equation is

$$\begin{aligned} & \underbrace{\left(\frac{\beta^2 - (r_2)^2}{r_2} \sin(r_2 l) - \frac{\beta^2 + (r_1)^2}{r_1} \frac{\cos(r_2 l)}{\cosh(r_1 l)} \sinh(r_1 l) \right)}_{(A)} \times \\ & \underbrace{\left(\frac{\beta^2 - (r_2)^2}{r_2} \cos(r_2 l) + \frac{\beta^2 + (r_1)^2}{r_1} \frac{\sin(r_2 l)}{\sinh(r_1 l)} \cosh(r_1 l) \right)}_{(B)} \\ & = 0 \end{aligned} \quad (27)$$

For $\omega^2 > \kappa GA/\rho I$, the frequency equation is

$$\begin{aligned} & \underbrace{\left(\frac{\beta^2 - (p_2)^2}{p_2} \sin(p_2 l) - \frac{\beta^2 - (p_1)^2}{p_1} \frac{\cos(p_2 l)}{\cos(p_1 l)} \sin(p_1 l) \right)}_{(C)} \times \\ & \underbrace{\left(\frac{\beta^2 - (p_2)^2}{p_2} \cos(p_2 l) - \frac{\beta^2 - (p_1)^2}{p_1} \frac{\sin(p_2 l)}{\sin(p_1 l)} \cos(p_1 l) \right)}_{(D)} \\ & = 0 \end{aligned} \quad (28)$$

Since the geometry and the boundary conditions of the beam are symmetric with respect to $x=0$, we can separate the natural modes of the beam into symmetric ones and anti-symmetric ones. Thus, we will derive them when $\omega^2 < \kappa GA/\rho I$ and when $\omega^2 > \kappa GA/\rho I$, one by one.

• When $\omega^2 < \kappa GA/\rho I$

Using the two boundary conditions of $W(-l) = W(l) = 0$, we rewrite Eq. (23) as follows

$$\begin{aligned} W(x) = & C \left(\sin(r_2 x) - \frac{\sin(r_2 l)}{\sinh(r_1 l)} \sinh(r_1 x) \right) \\ & + D \left(\cos(r_2 x) - \frac{\cos(r_2 l)}{\cosh(r_1 l)} \cosh(r_1 x) \right) \\ \Phi(x) = & -C \begin{Bmatrix} \frac{\beta^2 - (r_2)^2}{r_2} \cos(r_2 x) \\ + \frac{\beta^2 + (r_1)^2}{r_1} \frac{\sin(r_2 l)}{\sinh(r_1 l)} \cosh(r_1 x) \end{Bmatrix} \\ & + D \begin{Bmatrix} \frac{\beta^2 - (r_2)^2}{r_2} \sin(r_2 x) \\ - \frac{\beta^2 + (r_1)^2}{r_1} \frac{\cos(r_2 l)}{\cosh(r_1 l)} \sinh(r_1 x) \end{Bmatrix} \end{aligned} \quad (29)$$

If the boundary condition of $\Phi(l)=0$ satisfies ‘the factor (A) in Eq. (27) = 0’, the constant C in Eq. (29) vanishes. Thus, Eq. (29) can be written as follows

$$\begin{aligned} W(x) = & D \left(\cos(r_2 x) - \frac{\cos(r_2 l)}{\cosh(r_1 l)} \cosh(r_1 x) \right) \\ \Phi(x) = & D \begin{Bmatrix} \frac{\beta^2 - (r_2)^2}{r_2} \sin(r_2 x) \\ - \frac{\beta^2 + (r_1)^2}{r_1} \frac{\cos(r_2 l)}{\cosh(r_1 l)} \sinh(r_1 x) \end{Bmatrix} \end{aligned} \quad (30)$$

Since $W(x)$ in Eq. (30) is symmetric with respect to $x=0$, the corresponding natural mode is called symmetric mode in this paper though $\Phi(x)$ is anti-symmetric. The corresponding normalized modes are expressed as

$$\begin{Bmatrix} W_r^*(x) \\ \Phi_r^*(x) \end{Bmatrix} = \frac{1}{\sqrt{m_r}} \begin{Bmatrix} \cos(r_2 x) - \frac{\cos(r_2 l)}{\cosh(r_1 l)} \cosh(r_1 x) \\ \frac{(\beta_r)^2 - (r_{2r})^2}{r_{2r}} \sin(r_2 x) \\ - \frac{(\beta_r)^2 + (r_{1r})^2}{r_{1r}} \frac{\cos(r_2 l)}{\cosh(r_1 l)} \sinh(r_1 x) \end{Bmatrix} \quad (31)$$

where $m_r = \int_{-l}^l \left\{ \rho A (W_r(x)/D_r)^2 + \rho I (\Phi_r(x)/D_r)^2 \right\} dx$ and $r=1, 3, 5, \dots, n$. Since symmetric modes regularly occur before an anti-symmetric modes as natural frequency increases, the mode number of the symmetric modes, r is numbered as $r=1, 3, 5, \dots, n$, where n is an odd number.

If the boundary condition of $\Phi(l)=0$ satisfies ‘the factor (B) in Eq. (27) = 0’, the constant D in Eq. (29) vanishes. Therefore, Eq. (29) can be written as follows

$$W(x) = C \left(\sin(r_2 x) - \frac{\sin(r_2 l)}{\sinh(r_1 l)} \sinh(r_1 x) \right)$$

$$\Phi(x) = -C \begin{pmatrix} \frac{\beta^2 - (r_2)^2}{r_2} \cos(r_2 x) \\ + \frac{\beta^2 + (r_1)^2}{r_1} \frac{\sin(r_2 l)}{\sinh(r_1 l)} \cosh(r_1 x) \end{pmatrix} \quad (32)$$

Note that $W(x)$ in Eq. (32) is anti-symmetric with respect to $x=0$. The corresponding normalized anti-symmetric modes are

$$\begin{cases} W_r^*(x) \\ \Phi_r^*(x) \end{cases} = \frac{1}{\sqrt{m_r}} \begin{cases} \sin(r_2 x) - \frac{\sin(r_2 l)}{\sinh(r_1 l)} \sinh(r_1 x) \\ - \frac{(\beta_r)^2 - (r_{2r})^2}{r_{2r}} \cos(r_{2r} x) \\ - \frac{(\beta_r)^2 + (r_{1r})^2}{r_{1r}} \frac{\sin(r_{2r} l)}{\sinh(r_{1r} l)} \cosh(r_{1r} x) \end{cases} \quad (33)$$

where $m_r = \int_{-l}^l \left\{ \rho A (W_r(x)/C_r)^2 + \rho I (\Phi_r(x)/C_r)^2 \right\} dx$ and $r=2, 4, 6, \dots, m$. The mode number, m is an even number and m can be greater or less than n depending on a beam in hand.

• *When $\omega^2 > \kappa GA/\rho I$*

Using the similar manner, we can obtain symmetric and anti-symmetric eigenfunctions.

For the natural frequencies satisfying ‘{the factor (C) in Eq. (28)}=0’, we obtain the symmetric modes

$$\begin{aligned} W(x) &= H \left(\cos(p_2 x) - \frac{\cos(p_2 l)}{\cos(p_1 l)} \cos(p_1 x) \right) \\ \Phi(x) &= H \begin{pmatrix} \frac{\beta^2 - (p_2)^2}{p_2} \sin(p_2 x) \\ - \frac{\beta^2 - (p_1)^2}{p_1} \frac{\cos(p_2 l)}{\cos(p_1 l)} \sin(p_1 x) \end{pmatrix} \end{aligned} \quad (34)$$

The corresponding normalized modes are

$$\begin{cases} W_r^*(x) \\ \Phi_r^*(x) \end{cases} = \frac{1}{\sqrt{m_r}} \begin{cases} \cos(p_{2r} x) - \frac{\cos(p_{2r} l)}{\cos(p_{1r} l)} \cos(p_{1r} x) \\ \frac{(\beta_r)^2 - (p_{2r})^2}{p_{2r}} \sin(p_{2r} x) \\ - \frac{(\beta_r)^2 - (p_{1r})^2}{p_{1r}} \frac{\cos(p_{2r} l)}{\cos(p_{1r} l)} \sin(p_{1r} x) \end{cases} \quad (35)$$

where $m_r = \int_{-l}^l \left\{ \rho A (W_r(x)/H_r)^2 + \rho I (\Phi_r(x)/H_r)^2 \right\} dx$. The mode number, r cannot be specified because there does not exist a fixed regular pattern that symmetric or anti-symmetric mode appears as natural frequency increases.

For the natural frequencies satisfying ‘{the factor (D) in Eq. (28)}=0’, we obtain the anti-symmetric modes as follows

$$W(x) = G \left(\sin(p_2 x) - \frac{\sin(p_2 l)}{\sin(p_1 l)} \sin(p_1 x) \right)$$

$$\Phi(x) = -G \begin{pmatrix} \frac{\beta^2 - (p_2)^2}{p_2} \cos(p_2 x) \\ + \frac{\beta^2 - (p_1)^2}{p_1} \frac{\sin(p_2 l)}{\sin(p_1 l)} \cos(p_1 x) \end{pmatrix} \quad (36)$$

The corresponding anti-symmetric normalized modes are

$$\begin{cases} W_r^*(x) \\ \Phi_r^*(x) \end{cases} = \frac{1}{\sqrt{m_r}} \begin{cases} \sin(p_{2r} x) - \frac{\sin(p_{2r} l)}{\sin(p_{1r} l)} \sin(p_{1r} x) \\ - \frac{(\beta_r)^2 - (p_{2r})^2}{p_{2r}} \cos(p_{2r} x) \\ + \frac{(\beta_r)^2 - (p_{1r})^2}{p_{1r}} \frac{\sin(p_{2r} l)}{\sin(p_{1r} l)} \cos(p_{1r} x) \end{cases} \quad (37)$$

where $m_r = \int_{-l}^l \left\{ \rho A (W_r(x)/G_r)^2 + \rho I (\Phi_r(x)/G_r)^2 \right\} dx$.

2.2.3 Solution of dynamic displacements

Using the eigenvalues and the normalized modes, we can rewrite Eq. (18) as

$$([L] - \omega_r^2 [M]) \{V_r^*\} = \{0\}, \quad r = 1, 2, 3, \dots \quad (38)$$

where ω_r is the r -th natural frequency and the vector $\{V_r^*\}$ is the r -th normalized mode. The orthogonal conditions are (Lee and Lin 1998)

$$\begin{aligned} \int_{-l}^l \{V_r^*\}^T [M] \{V_s^*\} dx &= \delta_{rs}, \quad r, s = 1, 2, 3, \dots \\ \int_{-l}^l \{V_r^*\}^T [L] \{V_s^*\} dx &= \omega_r^2 \delta_{rs}, \quad r, s = 1, 2, 3, \dots \end{aligned} \quad (39)$$

where δ_{rs} is the Kronecker delta. The orthogonal conditions in Eq. (39) hold for the classical boundary conditions such as hinged end, fixed end and free end.

The solutions $w(x, t)$ and $\phi(x, t)$ can be expressed in the following eigenfunction expansion form

$$\begin{cases} w(x, t) \\ \phi(x, t) \end{cases} = \sum_{r=1}^{\infty} \begin{cases} W_r^*(x) \\ \Phi_r^*(x) \end{cases} \eta_r(t) \quad (40)$$

so that, inserting Eq. (40) into Eq. (12), we obtain

$$\begin{aligned} \sum_{r=1}^{\infty} [M] \begin{cases} W_r^*(x) \\ \Phi_r^*(x) \end{cases} \ddot{\eta}_r(t) + \sum_{r=1}^{\infty} [L] \begin{cases} W_r^*(x) \\ \Phi_r^*(x) \end{cases} \eta_r(t) \\ = \begin{cases} -\rho A \ddot{y}_s(x, t) \\ -\rho I \ddot{\theta}_s(x, t) \end{cases} \end{aligned} \quad (41)$$

Multiplying through by $\{W_r^*(x) \Phi_r^*(x)\}$, integrating over the domain, and considering the orthogonal conditions, we obtain the independent set of ordinary differential equations

$$\ddot{\eta}_r(t) + \omega_r^2 \eta_r(t) = Q_r(t), \quad r = 1, 2, 3, \dots \quad (42)$$

where

$$Q_r(t) = \int_{-l}^l [W_r^*(x) \quad \Phi_r^*(x)] \begin{Bmatrix} -\rho A \ddot{y}_s(x,t) \\ -\rho l \ddot{\theta}_s(x,t) \end{Bmatrix} dx \quad (43)$$

($r = 1, 2, 3, \dots$)

The response of Eq. (42) can be written as in the general form

$$\eta_r(t) = \frac{1}{\omega_r} \int_0^t Q_r(\tau) \cdot \sin \omega_r(t - \tau) d\tau + \eta_{r0} \cos \omega_r t + \frac{\dot{\eta}_{r0}}{\omega_r} \sin \omega_r t \quad (44)$$

where

$$\eta_{r0} = \int_{-l}^l [W_r^*(x) \quad \Phi_r^*(x)] [M] \begin{Bmatrix} w(x,0) \\ \phi(x,0) \end{Bmatrix} dx \quad (45)$$

($r = 1, 2, 3, \dots$)

and

$$\dot{\eta}_{r0} = \int_{-l}^l [W_r^*(x) \quad \Phi_r^*(x)] [M] \begin{Bmatrix} \dot{w}(x,0) \\ \dot{\phi}(x,0) \end{Bmatrix} dx \quad (46)$$

($r = 1, 2, 3, \dots$)

Inserting Eq. (44) into Eq. (40), we obtain the general response of the dynamic components

$$\begin{Bmatrix} w(x,t) \\ \phi(x,t) \end{Bmatrix} = \sum_{r=1}^{\infty} \begin{Bmatrix} W_r^*(x) \\ \Phi_r^*(x) \end{Bmatrix} \left(\frac{1}{\omega_r} \int_0^t Q_r(\tau) \cdot \sin \omega_r(t - \tau) d\tau + \eta_{r0} \cos \omega_r t + \frac{\dot{\eta}_{r0}}{\omega_r} \sin \omega_r t \right) \quad (47)$$

2.3 Total responses

2.3.1 Total displacements

Inserting Eq. (47) into Eq. (5), we obtain the total displacements

$$\begin{Bmatrix} y(x,t) \\ \theta(x,t) \end{Bmatrix} = \begin{Bmatrix} y_s(x,t) \\ \theta_s(x,t) \end{Bmatrix} + \sum_{r=1}^{\infty} \begin{Bmatrix} W_r^*(x) \\ \Phi_r^*(x) \end{Bmatrix} \left(\frac{1}{\omega_r} \int_0^t Q_r(\tau) \cdot \sin \omega_r(t - \tau) d\tau + \eta_{r0} \cos \omega_r t + \frac{\dot{\eta}_{r0}}{\omega_r} \sin \omega_r t \right) \quad (48)$$

Using the quasi-static displacements in Eq. (8), $Q_r(t)$ in Eq. (43) is expressed as follows

$$Q_r(t) = \tilde{A}_r \ddot{a}(t) + \tilde{B}_r \ddot{b}(t), \quad r = 1, 2, 3, \dots \quad (49)$$

where

$$\tilde{A}_r = - \left(\rho A \int_{-l}^l W_r^*(x) \cdot L_1(x) dx + \rho l \int_{-l}^l \Phi_r^*(x) \cdot R_1(x) dx \right) \quad (50)$$

$$\tilde{B}_r = - \left(\rho A \int_{-l}^l W_r^*(x) \cdot L_2(x) dx + \rho l \int_{-l}^l \Phi_r^*(x) \cdot R_2(x) dx \right)$$

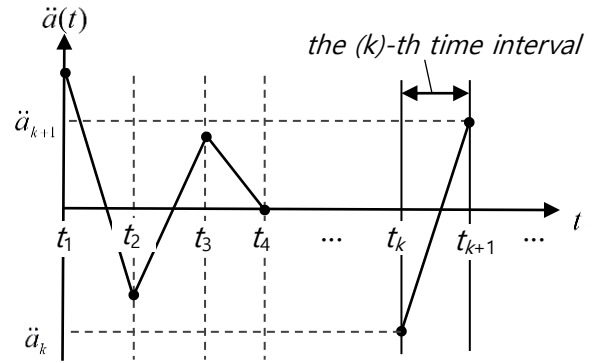


Fig. 3 Time history of support acceleration given in the form of a set of piecewise linear functions

By using Eq. (49), the term of $\int_0^t Q_r(\tau) \cdot \sin \omega_r(t - \tau) d\tau$ contained in Eq. (44) is expressed as

$$\int_0^t Q_r(\tau) \cdot \sin \omega_r(t - \tau) d\tau = \tilde{A}_r \int_0^t \ddot{a}(\tau) \cdot \sin \omega_r(t - \tau) d\tau + \tilde{B}_r \int_0^t \ddot{b}(\tau) \cdot \sin \omega_r(t - \tau) d\tau \quad (51)$$

which requires the time histories of support accelerations, $\ddot{a}(t)$ and $\ddot{b}(t)$.

Suppose the seismic waves or the support motions are recorded in terms of acceleration at discrete time points and thus the time histories of acceleration can be described by a set of piecewise linear functions as shown in Fig. 3. Then the support motions in the (k) -th time interval can be expressed as follows

$$\begin{cases} \ddot{a}^{(k)}(t) = A_1^{(k)} t + B_1^{(k)} \\ \dot{a}^{(k)}(t) = \frac{1}{2} A_1^{(k)} t^2 + B_1^{(k)} t + C_1^{(k)} \\ a^{(k)}(t) = \frac{1}{6} A_1^{(k)} t^3 + \frac{1}{2} B_1^{(k)} t^2 + C_1^{(k)} t + D_1^{(k)} \end{cases} \quad \text{and} \quad (52)$$

$$\begin{cases} \ddot{b}^{(k)}(t) = A_2^{(k)} t + B_2^{(k)} \\ \dot{b}^{(k)}(t) = \frac{1}{2} A_2^{(k)} t^2 + B_2^{(k)} t + C_2^{(k)} \\ b^{(k)}(t) = \frac{1}{6} A_2^{(k)} t^3 + \frac{1}{2} B_2^{(k)} t^2 + C_2^{(k)} t + D_2^{(k)} \end{cases}$$

where $A_1^{(k)}$, $B_1^{(k)}$, $A_2^{(k)}$ and $B_2^{(k)}$ ($k = 1, 2, 3, \dots$) are

$$A_1^{(k)} = \frac{\ddot{a}_{k+1} - \ddot{a}_k}{t_{k+1} - t_k},$$

$$B_1^{(k)} = \ddot{a}_k - \frac{\ddot{a}_{k+1} - \ddot{a}_k}{t_{k+1} - t_k} t_k,$$

$$\begin{aligned} A_2^{(k)} &= \frac{\ddot{b}_{k+1} - \ddot{b}_k}{t_{k+1} - t_k}, \\ B_2^{(k)} &= \ddot{b}_k - \frac{\ddot{b}_{k+1} - \ddot{b}_k}{t_{k+1} - t_k} t_k \end{aligned} \quad (53)$$

The coefficients of $C_i^{(1)}$ and $D_i^{(1)}$ ($i=1, 2$) are determined by the initial conditions in Eq. (4), and $C_i^{(k)}$ and $D_i^{(k)}$ ($i=1, 2; k=2, 3, 4, \dots$) are determined successively by following relations

$$\begin{aligned} C_i^{(k)} &= \frac{1}{2} A_i^{(k-1)} t_k^2 + B_i^{(k-1)} t_k + C_i^{(k-1)} \\ &\quad - \left(\frac{1}{2} A_i^{(k)} t_k^2 + B_i^{(k)} t_k \right) \\ D_i^{(k)} &= \frac{1}{6} A_i^{(k-1)} t_k^3 + \frac{1}{2} B_i^{(k-1)} t_k^2 + C_i^{(k-1)} t_k + D_i^{(k-1)} \\ &\quad - \left(\frac{1}{6} A_i^{(k)} t_k^3 + \frac{1}{2} B_i^{(k)} t_k^2 + C_i^{(k)} t_k \right) \end{aligned} \quad (54)$$

Using the support displacements $a^{(k)}(t)$ and $b^{(k)}(t)$ in Eq. (52), we can calculate the quasi-static displacements in Eq. (8). Using $\ddot{a}^{(k)}(t)$ and $\ddot{b}^{(k)}(t)$ in Eq. (52), we can also express Eq. (51) as follows when the current time t is within the (k)-th time interval, i.e. $t_k \leq t \leq t_{k+1}$

$$\begin{aligned} &\int_0^t Q_r(\tau) \cdot \sin \omega_r(t-\tau) d\tau \\ &= \tilde{A}_r \left\{ \sum_{m=1}^{k-1} \int_{t_m}^{t_{m+1}} (A_1^{(m)} \tau + B_1^{(m)}) \cdot \sin \omega_r(t-\tau) d\tau \right. \\ &\quad \left. + \int_{t_k}^t (A_1^{(k)} \tau + B_1^{(k)}) \cdot \sin \omega_r(t-\tau) d\tau \right\} \\ &+ \tilde{B}_r \left\{ \sum_{m=1}^{k-1} \int_{t_m}^{t_{m+1}} (A_2^{(m)} \tau + B_2^{(m)}) \cdot \sin \omega_r(t-\tau) d\tau \right. \\ &\quad \left. + \int_{t_k}^t (A_2^{(k)} \tau + B_2^{(k)}) \cdot \sin \omega_r(t-\tau) d\tau \right\} \end{aligned} \quad (55)$$

Finally, we can calculate the total displacement in Eq. (48) for a set of time histories of seismic accelerations or support motions.

2.3.2 Bending moment and shear force

Using Eq. (8) and Eq. (48), we can rewrite the bending moment and the shear force in Eq. (2) as

$$\begin{aligned} M_{total}(x, t) &= M_{static}(x, t) + M_{dynamic}(x, t) \\ Q_{total}(x, t) &= Q_{static}(x, t) + Q_{dynamic}(x, t) \end{aligned} \quad (56)$$

where M_{static} and Q_{static} denote static component of bending moment and static part of shear force, respectively, and $M_{dynamic}$ and $Q_{dynamic}$ denote dynamic components. They are expressed as follows

$$M_{static}(x, t) = EI \left(a(t) \cdot \frac{dR_1(x)}{dx} + b(t) \cdot \frac{dR_2(x)}{dx} \right) \quad (57)$$

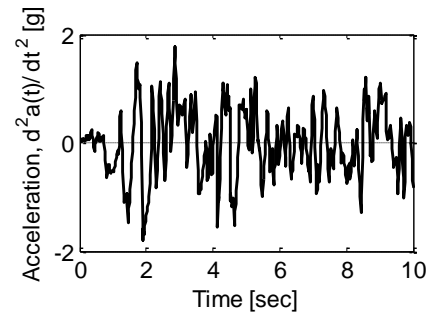
$$M_{dynamic}(x, t) = EI \sum_{r=1}^{\infty} \frac{d\Phi_r^*(x)}{dx} \eta_r(t) \quad (58)$$

$$Q_{static}(x, t) = \kappa GA \left\{ \begin{aligned} &a(t) \cdot \left(\frac{dL_1(x)}{dx} - R_1(x) \right) \\ &+ b(t) \cdot \left(\frac{dL_2(x)}{dx} - R_2(x) \right) \end{aligned} \right\} \quad (59)$$

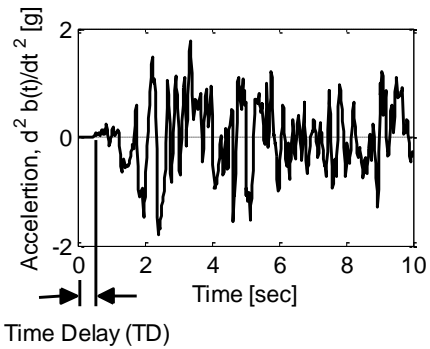
$$Q_{dynamic}(x, t) = \kappa GA \sum_{r=1}^{\infty} \left(\frac{dW_r^*(x)}{dx} - \Phi_r^*(x) \right) \eta_r(t) \quad (60)$$

3. Application examples and discussions

To illustrate the vibration of Timoshenko beam excited by different support motions at ends, the first 10 sec of the 1940 El Centro Earthquake accelerogram (E-W component) have been used as input support motions. To model asynchronous or different support excitations as shown in Fig. 4, it is assumed that the earthquake travelling waves originate from the left and propagate longitudinally to the right at the speed of 100 m/s. The wave velocity is quite low compared with an actual one but the computed results



(a) Prescribed time history of acceleration at the left support



(b) Prescribed time history of acceleration at the right support

Fig. 4 The fixed-fixed beam in Fig. 2 is subjected to the accelerations, $d^2\{a(t)\}/dt^2$ and $d^2\{b(t)\}/dt^2$ at the left end and the right end, respectively

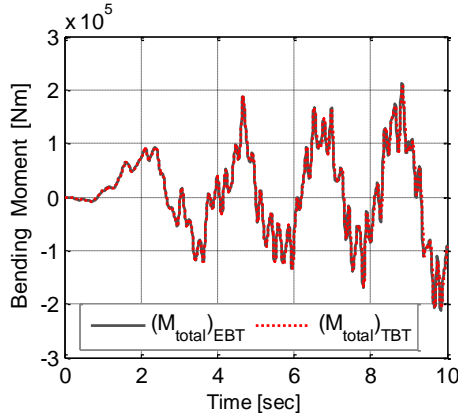
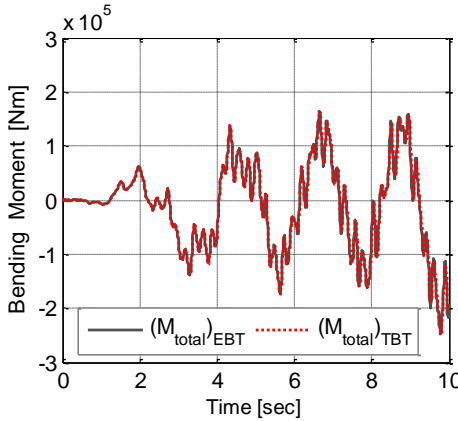
(a) Bending moment at $x=-30$ m(b) Bending moment at $x=30$ m

Fig. 5 Comparison of time histories of bending moment of the slender beam (TD=0.60 sec)

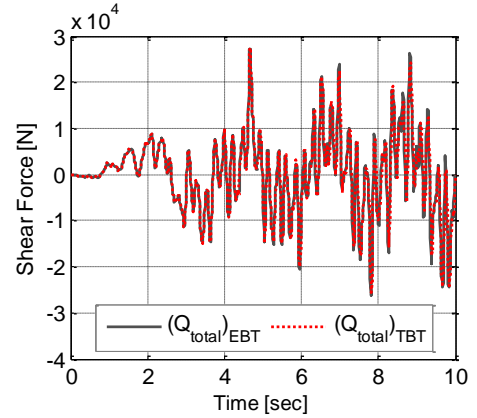
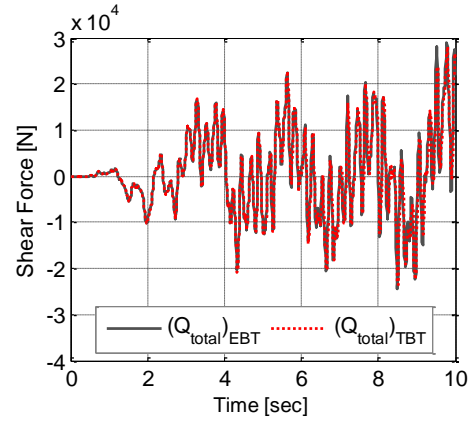
(a) Shear force at $x=-30$ m(b) Shear force at $x=30$ m

Fig. 6 Comparison of time histories of shear forces of the slender beam (TD=0.60 sec)

are useful to develop an understanding of the structural behavior. The time delay, TD, is computed from $TD = (\text{span length}) / (\text{wave velocity})$.

The input data for the beams with the section of hollow circle are as follows: $E=200$ GPa, $\rho=7860$ kg/m³, $\nu=0.3$, outer diameter $d_o=0.32$ m, inner diameter $d_i=0.22$ m, and shear correction factor $\kappa = \{6(1+\nu)(1+f^2)^2\} / \{7+6\nu(1+f^2)^2 + (20+12\nu)f^2\}$ where $f=d_i/d_o$ (Blevins, 1979). The lengths are: $L=60$ m for a slender beam and $L=2$ m for a stocky beam, respectively. The time delay for the 60 m long beam is 0.60 sec and that for the 2 m long beam is 0.02 sec.

All the responses are calculated by using the first ten modes of each beam throughout this paper because they yield sufficiently converged solutions. The natural frequencies used in the slender beam are much lower than the critical frequency of $\omega_c = (\kappa GA / \rho I)^{0.5}$ while the first seven frequencies of the stocky beam are lower than ω_c and the rest of them are higher than ω_c .

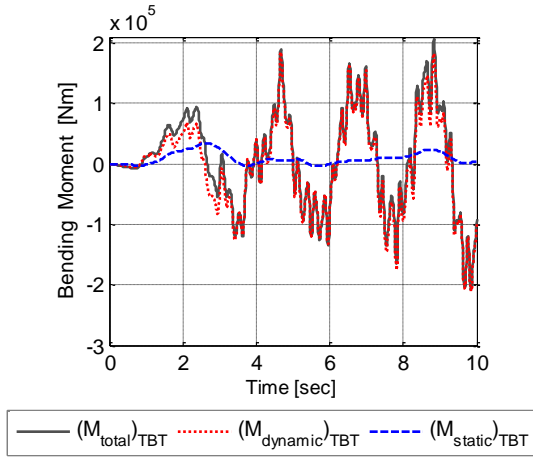
3.1 Numerical simulation for the slender beam

To check the correctness of the proposed method, the calculations for the slender beam of length 60 m are carried out by using Euler-Bernoulli beam theory (EBT) (Chen *et al.* 1996) as well as Timoshenko beam theory (TBT) and the results are to be compared. It is expected that the two

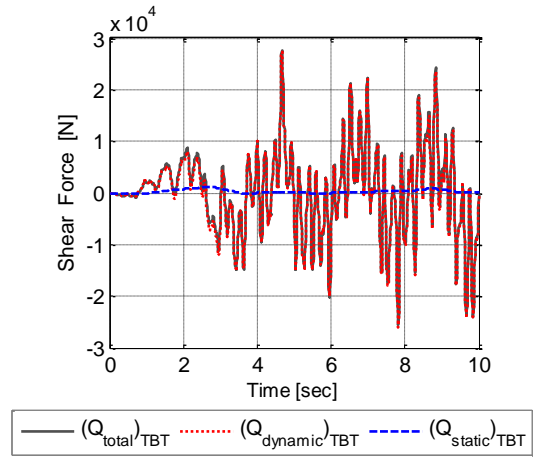
responses of the slender beam are nearly identical because the effects of rotary inertia and shear deformation of the slender beam are so small that they can be neglected.

Since the bending moment and the shear force are main concerns in structural design, their time histories due to the support motions are plotted in Fig. 5 and Fig. 6, respectively. The reason that the time histories at the ends are presented in Fig. 5 and Fig. 6 is that the maximal structural loads may occur at ends in the fixed-fixed beam. Fig. 5 and Fig. 6 show when the maximums of the structural loads occur at ends. They also show that the results based on TBT agree with those based on EBT well.

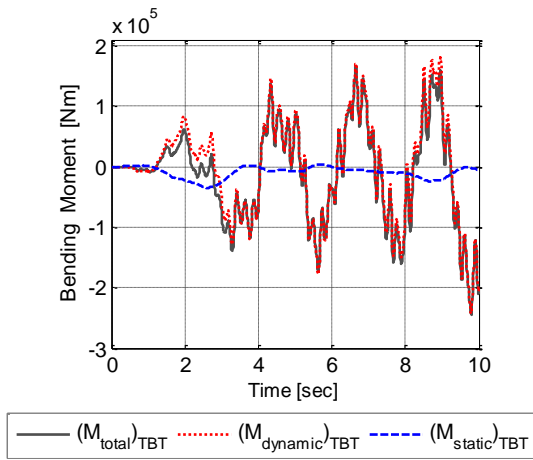
Decomposing the bending moment ($(M_{total})_{TBT}$) and the shear force ($(Q_{total})_{TBT}$) at $x=\pm 30$ m into their static components ($(M_{static})_{TBT}$ and $(Q_{static})_{TBT}$) and dynamic components ($(M_{dynamic})_{TBT}$ and $(Q_{dynamic})_{TBT}$), we plotted them in Fig. 7 and Fig. 8, respectively. Fig. 7 and Fig. 8 show that the magnitudes of static components are small compared with the corresponding dynamic components, i.e., the magnitudes of M_{total} and Q_{total} are governed by their dynamic components. Such kind of beams are called 'dynamic component-dominated beam (DCD beam)' in this paper. According to author's experience, the lower the fundamental frequency is and the larger the slenderness ratio of $s (=L/r)$, where r is radius of gyration is, the more dominant the dynamic components become. In this



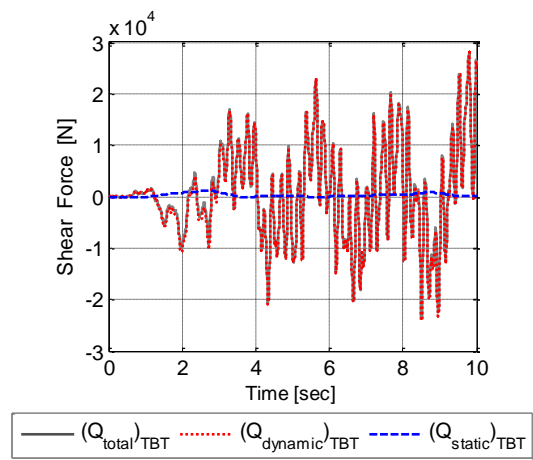
(a) Bending moment at $x=-30$ m



(a) Shear force at $x=-30$ m



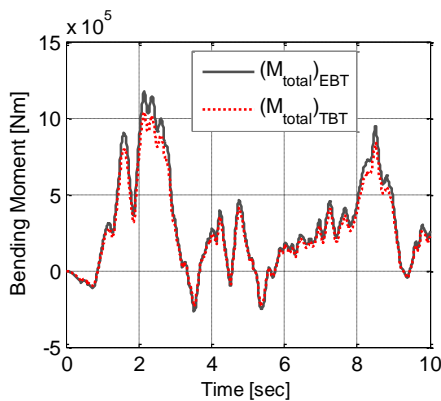
(b) Bending moment at $x=30$ m



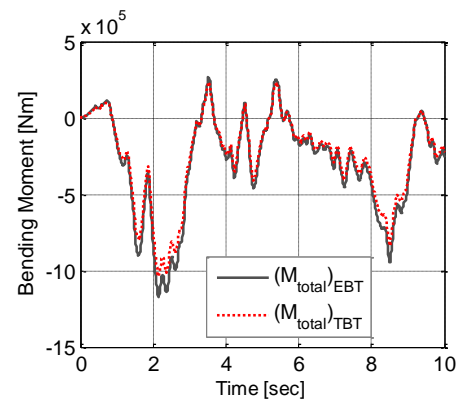
(b) Shear force at $x=30$ m

Fig. 7 M_{total} , M_{static} and $M_{dynamic}$ in the slender beam when $TD=0.60$ sec

Fig. 8 Q_{total} , Q_{static} and $Q_{dynamic}$ in the slender beam when $TD=0.60$ sec



(a) Bending moment at $x=-1$ m



(b) Bending moment at $x=1$ m

Fig. 9 Comparison of time histories of bending moments of the stocky beam ($TD=0.02$ sec)

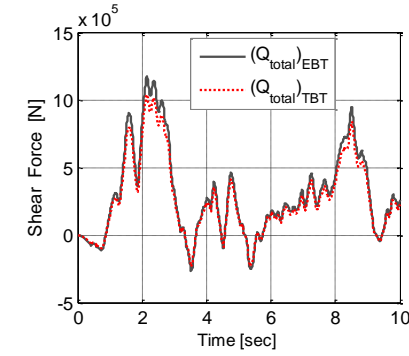
example, the fundamental frequency is 3.0425 [rad/s] and the slenderness ratio is 618.03.

3.2 Numerical simulation for the stocky beam

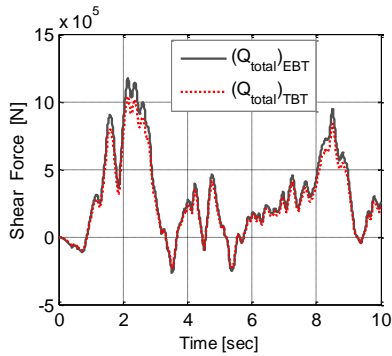
Consider the fixed-fixed stocky beam of span length 2 m, which belongs to an extreme case of a thick beam. The time

histories of bending moment and shear force at $x=\pm 1$ m caused by the support motions are plotted in Fig. 9 and Fig. 10, respectively. Fig. 9 and Fig. 10 show that the results based on TBT do not agree with those based on EBT. This is because the Euler-Bernoulli beam theory does not take account of the effect of rotary inertia and shear deformation.

Decomposing $(M_{total})_{TBT}$ and $(Q_{total})_{TBT}$ at $x=\pm 1$ m into

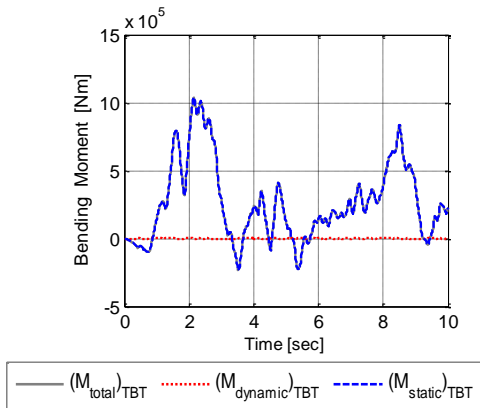


(a) Shear force at $x=-1$ m

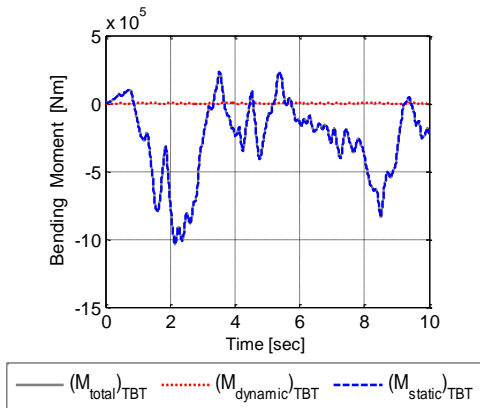


(b) Shear force at $x=1$ m

Fig. 10 Comparison of time histories of shear forces of the stocky beam (TD=0.02 sec)

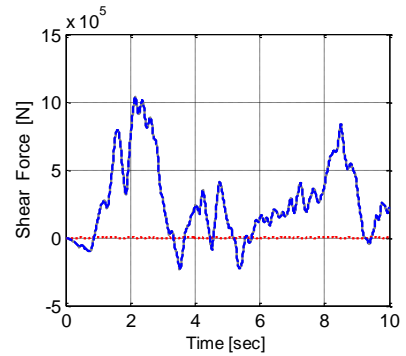


(a) Bending moment at $x=-1$ m

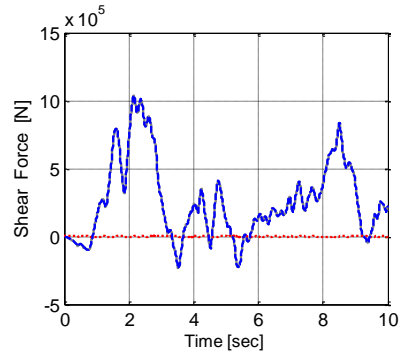


(b) Bending moment at $x=1$ m

Fig. 11 M_{total} , M_{static} and $M_{dynamic}$ in the stocky beam (TD=0.02 sec)



(a) Shear force at $x=-1$ m



(b) Shear force at $x=1$ m

Fig. 12 Q_{total} , Q_{static} and $Q_{dynamic}$ in the stocky beam (TD=0.02 sec)

static components and dynamic components, respectively, we plotted them in Fig. 11 and Fig. 12. Fig. 11 and Fig. 12 show that the magnitudes of M_{total} and Q_{total} are governed by their static components, that is, the static components are very large compared with the dynamic components and thus the dynamic components can be neglected. This contrasts with the behavior of the slender beam considered in the previous section. This kind of beams are called ‘static component-dominated beam (SCD beam)’ in this paper.

According to author’s experience, the higher the fundamental frequency of a beam is and the smaller the slenderness ratio is, the more dominant the static components become. In this example, the fundamental frequency is 2189.4 [rad/s] and the slenderness ratio is 20.601.

3.3 Bending moment and shear force affected by the time delay

Since $M_{dynamic}$ and $Q_{dynamic}$ of the stocky beam or SCD beam are so small compared with the static components (M_{static} and Q_{static}), M_{total} and Q_{total} can be calculated easily only by static components, without dynamic analysis. Thus, from Eqs. (8)-(10), Eq. (57) and Eq. (59), we have

$$M_{total}(x,t) \cong M_{static}(x,t) = \frac{3EI}{2l^2} \frac{1}{1+3K} \{a(t) - b(t)\}x \quad (61)$$

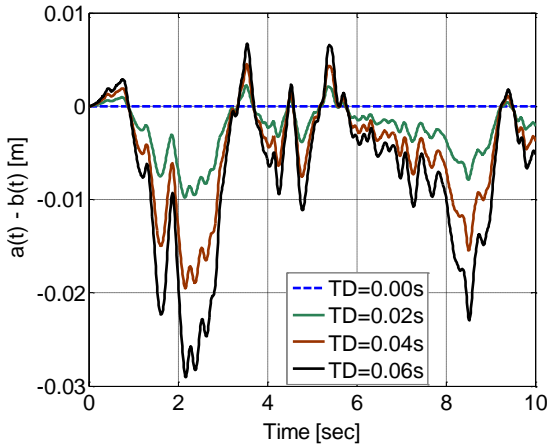


Fig. 13 Time history of $a(t)-b(t)$ affected by time delay (TD)

and

$$Q_{total}(x,t) \cong Q_{static}(t) = -\frac{3\kappa GA}{2l} \{a(t) - b(t)\} \quad (62)$$

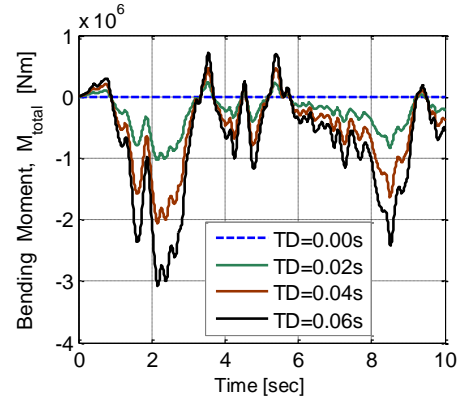
The above equations state that the magnitudes of bending moment and shear force are proportional to the difference between support displacements, $a(t)-b(t)$. We plotted $a(t)-b(t)$ in Fig. 13 for different time delays, which shows that different TD produces different time history of $a(t)-b(t)$ and the magnitude of $|a(t)-b(t)|$ increases as the time delay (TD) increases. This implies that the magnitudes of bending moment and shear force increase as the wave velocity decreases.

For the stocky beam, the time histories of total bending moment and total shear force at $x=1$ m are plotted in Fig. 14(a) and Fig. 14(b) for four different TD's, which show that the magnitudes of bending moment and shear force increase as the TD increases. The maximal magnitudes are $(M_{total})_{max} \approx 3 \times 10^6$ Nm and $(Q_{total})_{max} \approx 3 \times 10^6$ N, respectively when TD=0.06 sec. But the maximal magnitudes of dynamic components in the corresponding time histories at the same location are $(M_{dynamic})_{max} \approx 200$ Nm and $(Q_{dynamic})_{max} \approx 500$ N, respectively.

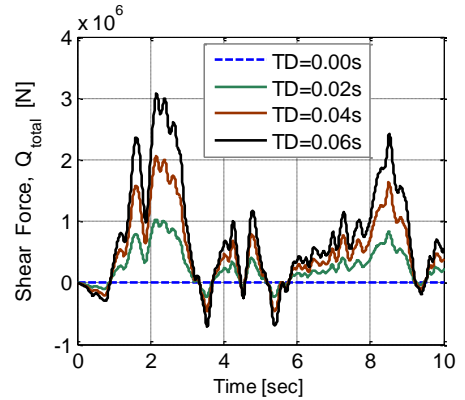
Fig. 13 and Fig. 14 show the following facts: (i) There is a similarity between the pattern of the time history of $a(t)-b(t)$ in Fig. 13 and the pattern of the time histories of M_{total} and Q_{total} in Fig. 14 for each TD. (ii) The maximal magnitudes of $|M_{total}|$ and $|Q_{total}|$ occur at the time that the maximal magnitude of $|a(t)-b(t)|$ occurs. (iii) $|M_{total}|$ and $|Q_{total}|$ are minimal when TD=0.0. These facts are closely related to the facts that M_{total} and Q_{total} are governed by M_{static} and Q_{static} , respectively and that their magnitudes are proportional to $|a(t)-b(t)|$ as explained in Eqs. (61) and (62).

4. Conclusions

This study proposes an analytic method based on Timoshenko beam theory to predict the bending moment and the shear force of the beam subjected to support motions. The analytic responses of a fixed-fixed beam subjected to a real seismic support motions are illustrated to



(a) Bending moment at $x=1$ m



(b) Shear force at $x=1$ m

Fig. 14 Time histories of bending moment and shear force of the stocky beam affected by time delay (TD)

show the principled approach to the proposed method since fixed-fixed thick beams are frequently used in nuclear power plants. The results of the dynamic analysis are useful to develop an understanding of the structural behavior of the beam, and they are as follows:

- In the DCD (dynamic component-dominated) beam such as the slender beam considered in this paper, the total moment and the total shear force are governed by the dynamic components, that is, the static components of the structural load are small compared with the dynamic components.
- In the SCD (static component-dominated) beam such as the stocky beam considered in this paper, the total moment and the total shear force are governed by the static components, that is, the static components of the structural load are very large compared with the dynamic components. Thus, the dynamic components can be neglected. Therefore, it is possible to estimate bending moment and shear force without dynamic analysis in SCD beam.
- In the SCD beam, the magnitudes of bending moment and shear force are proportional to the difference between support displacements. For this reason, the maximal magnitudes of bending moment and shear force vary as the TD changes. In other words, the maximal magnitudes of structural loads vary depending on the wave velocity. In this paper, we omitted mentioning the

following fact with an appropriate parameter in detail: The higher the fundamental frequency of a beam is and the smaller the slenderness ratio is, the more dominant the static components become. Further researches on an appropriate parameter to define SCD beam are required to utilize the feature in a structural design without dynamic analysis.

References

- Abdel-Ghaffar, A.M. and Rood, J.D. (1982), "Simplified earthquake analysis of suspension bridge towers", *J. Eng. Mech. Div.*, ASCE, **108**(EM2), 291-302.
- Blevins, R.D. (1979), *Formulas for Natural Frequency and Mode Shape*, Van Nostrand Reinhold Company, New York, NY, USA.
- Chen, J.T., Hong, H.K., Yeh, C.S. and Chyuan, S.W. (1996), "Integral representations and regularizations for a divergent series solution of a beam subjected to support motions", *Earthq. Eng. Struct. Dyn.*, **25**, 909-925.
- Chopra, A.K. (1995), *Dynamics of Structures: Theory and Application to Earthquake Engineering*, Prentice Hall, USA.
- Clough, R.W. and Penzien, J. (1993), *Dynamics of Structures*, 2nd Edition, McGraw-Hill, Singapore.
- Datta, T.K. (2010), *Seismic Analysis of Structures*, John Wiley & Sons (Asia) Pte Ltd, Singapore.
- Díaz-de-Anda, A., Flores, J., Gutiérrez, L., Méndez-Sánchez, R.A. and Monsivais, G. (2012), "Experimental study of the Timoshenko beam theory predictions", *J. Sound Vib.*, **331**, 5732-5744.
- Fryba, L. and Yau, J.D. (2009), "Suspended bridges subjected to moving loads and support motions due to earthquake", *J. Sound Vib.*, **319**, 218-227.
- Han, S.M., Benaroya, H. and Wei, T. (1999), "Dynamics of transversely vibrating beams using four engineering theories", *J. Sound Vib.*, **225**(3), 935-988.
- Kim, Y.W. (2015), "Finite element formulation for earthquake analysis of single-span beams involving forced deformation caused by multi-support motions", *J. Mech. Sci. Technol.*, **29**(2), 461-469.
- Kim, Y.W. (2016), "Dynamic analysis of Timoshenko beam subjected to support motions", *J. Mech. Sci. Technol.*, **30**(2), 4167-4176.
- Kim, Y.W. and Jung, M.J. (2013), "Moving support elements for dynamic finite element analysis of statically determinate beams subjected to support motions", *Tran. Korean Soc. Mech. Eng. A*, **37**(4), 555-567.
- Lee, S.Y. and Lin, S.M. (1998), "Non-uniform Timoshenko beams with time-dependent elastic boundary conditions", *J. Sound Vib.*, **217**(9), 223-238.
- Li, X.Y., Zhao, X. and Li, Y.H. (2014), "Green's function of the forced vibration of Timoshenko beams with damping effect", *J. Sound Vib.*, **333**, 1781-1795.
- Liu, M.F., Chang, T.P. and Zeng, D.Y. (2011), "The interactive vibration in a suspension bridge system under moving vehicle loads and vertical seismic excitations", *Appl. Math. Model.*, **35**, 398-411.
- Majkut, L. (2009), "Free and forced vibrations of Timoshenko beams described by single difference equation", *J. Theor. Appl. Mech.*, **47**(1), 193-210.
- Masri, S.F. (1976), "Response of beam to propagating boundary excitation", *Earthq. Eng. Struct. Dyn.*, **4**, 497-509.
- Mindlin, R.D. and Goodman, L.E. (1950), "Beam vibrations with time-dependent boundary conditions", *J. Appl. Mech.*, ASME, **17**, 377-380.
- Stephen, N.G. and Puchegger, S. (2006), "On valid frequency range of Timoshenko beam theory", *J. Sound Vib.*, **297**, 1082-1087.
- van Rensburg, N.F.J. and van der Merwe, A.J. (2006), "Natural frequencies and modes of a Timoshenko beam", *Wave Motion*, **44**, 58-69.
- Yau, J.D. (2009), "Dynamic response analysis of suspended beams subjected to moving vehicles and multiple support excitations", *J. Sound Vib.*, **325**, 907-922.
- Yau, J.D. and Fryba, L. (2007), "Response of suspended beams due to moving loads and vertical seismic ground excitations", *Eng. Struct.*, **29**, 3255-3262.
- Zhang, Y.H., Li, Q.S., Lin, J.H. and Williams, F.W. (2009), "Random vibration analysis of long-span structures subjected to spatially varying ground motions", *Soil Dyn. Earthq. Eng.*, **29**, 620-629.

CC